SUPPLEMENTARY INFORMATION

Role of Spacer Cations and Structural Distortion in Two-Dimensional Germanium Halide Perovskites

Rossella Chiara,[a] Marta Morana,[a,] Massimo, Boiocchi,[b] Mauro Coduri,[a] Marinella Striccoli,[c] Francesco Fracassi,[c] Andrea Listorti,[c] Arup Mahata,[d,e] Paolo Quadrelli,[a] Mattia Gaboardi,[f] Chiara Milanese,[a] Luca Bindi,[g] Filippo De Angelis,[d,e,h] Lorenzo Malavasi[a,*]*

[a]Department of Chemistry and INSTM, University of Pavia, Via Taramelli 16, Pavia, 27100, Italy

[b]Centro Grandi Strumenti (CGS), University of Pavia, Via Bassi 21, Pavia, 27100, Italy

[c]Department of Chemistry, University of Bari "Aldo Moro", via Orabona 4, 70126, Bari, Italy

[d]Computational Laboratory for Hybrid/Organic Photovoltaics (CLHYO), Istituto CNR di Scienze e Tecnologie Chimiche "Giulio Natta" (CNR-SCITEC), Via Elce di Sotto 8, 06123 Perugia, Italy

[e]CompuNet, Istituto Italiano di Tecnologia, Via Morego 30, 16163 Genova, Italy

[f]Elettra-Sincrotrone Trieste S.C.p.A., S.S. 14 km 163.5 in Area Science Park, Basovizza, 34149, Trieste, Italy

[g]Dipartimento di Scienze della Terra, Università degli Studi di Firenze, Via G. La Pira 4, 50121 Firenze, Italy

[h]Department of Chemistry, Biology and Biotechnology, University of Perugia, Via Elce di Sotto 8, 06123 Perugia, Italy

Fig 1S – Images of single crystals of a) PEA$_2$GeBr$_4$, b) BZA$_2$GeBr$_4$, c) BrPEA$_2$GeBr$_4$, and d) FPEA$_2$GeBr$_4$.
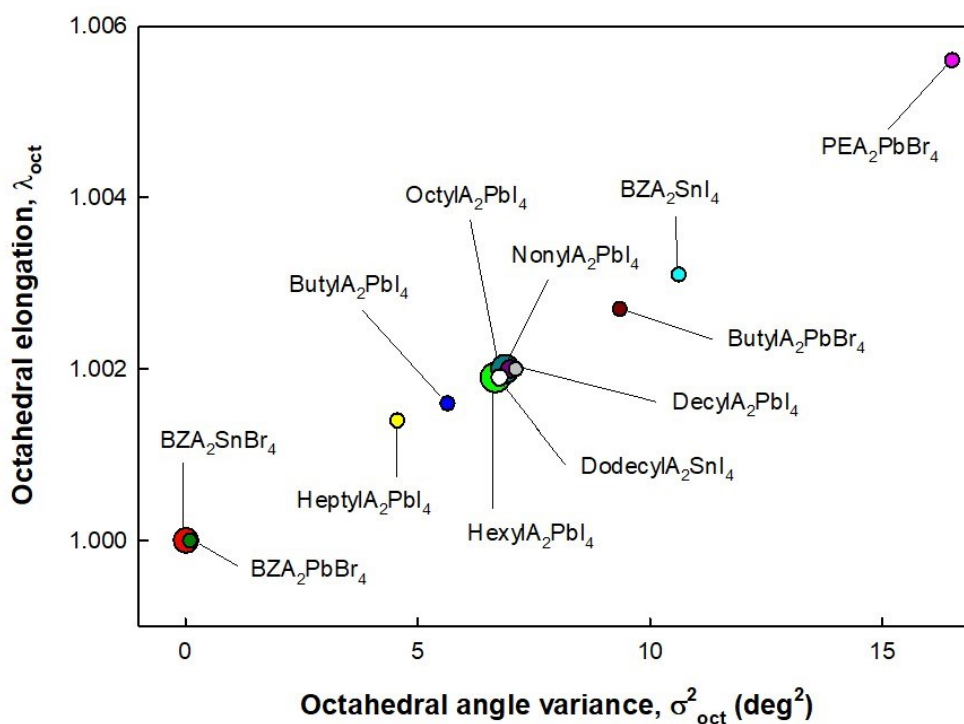
Fig 2S - Octahedral distortion parameters for different hybrid perovskites compositions. Data taken from ref 1.[1]

Table 1S - Distortion parameters RT for PEA_2GeBr_4, $BrPEA_2GeBr_4$, $FPEA_2GeBr_4$, and BZA_2GeBr_4 at room temperature
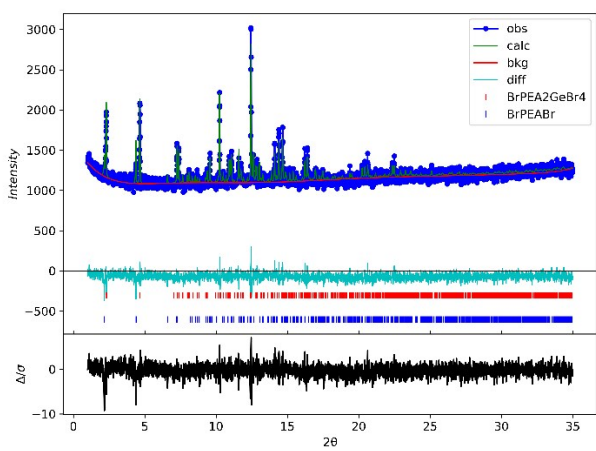
	Average bond length Å	Polyhedral Volume Å^3	Distortion index	Quadratic elongation	Bond angle variance degrees^2	Ge-Br-Ge Angle degrees
PEA_2GeBr_4	2.9365	33.4205	0.1326	1.0245	23.5846	157.82
$BrPEA_2GeBr_4$	2.9301	32.3641	0.1111	1.0369	79.4978	156.37
$FPEA_2GeBr_4$	2.9299	33.2686	0.1258	1.0213	18.9101	157.94
BZA_2GeBr_4	2.9123	32.6517	0.1185	1.0202	18.4717	155.27

A   **B**
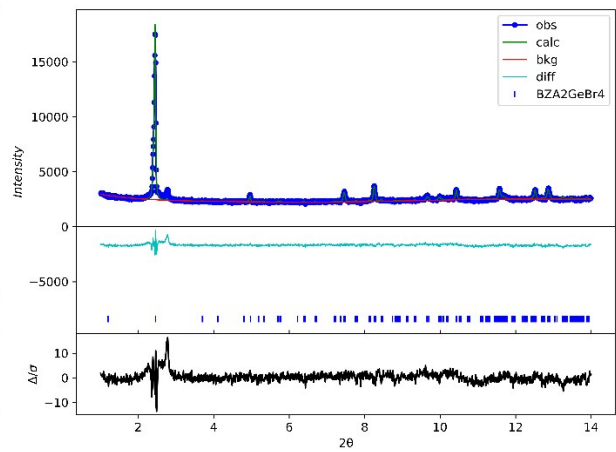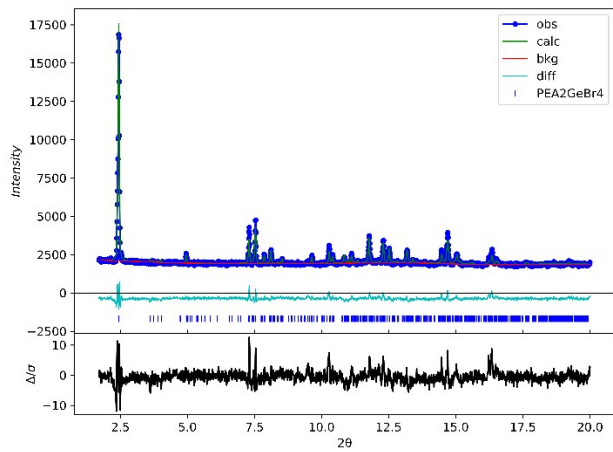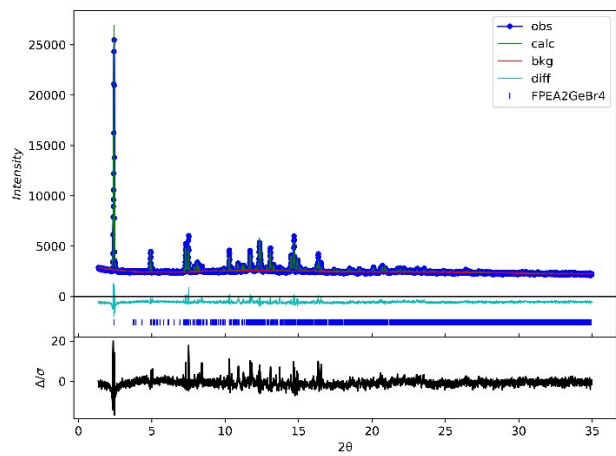
Fig 3S – Exemplary Rietveld refinements of the RT SXRD data for a) PEA$_2$GeBr$_4$, b) BZA$_2$GeBr$_4$, c) BrPEA$_2$GeBr$_4$, and d) FPEA$_2$GeBr$_4$.
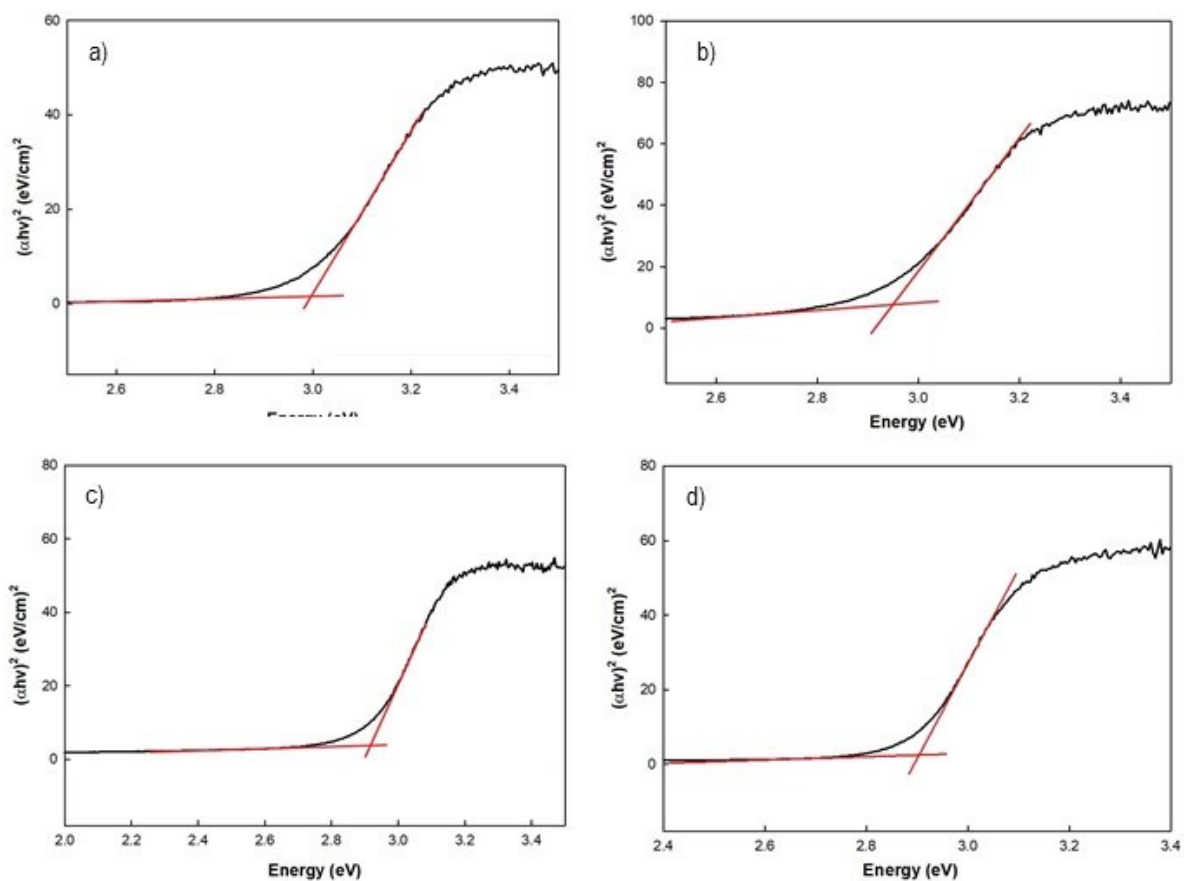
Figure 4S. Tauc plots of a) PEA_2GeBr_4, b) $BrPEA_2GeBr_4$, c) $FPEA_2GeBr_4$ and d) BZA_2GeBr_4.

Table 2S - Distortion parameters for PEA_2GeBr_4, $FPEA_2GeBr_4$, and BZA_2GeBr_4 at 100 K

	Average bond length Å	Polyhedral Volume Å^3	Distortion index	Quadratic elongation	Bond angle variance degrees^2	Ge-Br-Ge Angle degrees
PEA_2GeBr_4	2.9212	32.9271	0.1271	1.0225	21.6474	157.37
$FPEA_2GeBr_4$	2.9299	32.7452	0.1249	1.0207	17.9598	157.60
BZA_2GeBr_4	2.8999	32.2786	0.1167	1.0191	15.3505	155.02

Experimental methods:

Single crystal synthesis:

Single crystals were prepared by a solution method under inert atmosphere. The general procedure consisted in the dissolution of a proper amount of GeO_2 powder in a large excess of 48% w/w aqueous HBr in the presence of hypophosphorous acid (50% w/w aqueous H_3PO_2), in order to reduce Ge(IV) to Ge(II) and to stabilize the reduced oxidation state of germanium. The solution was maintained under continuous stirring and nitrogen atmosphere in order to prevent Ge oxidation. Then, the solution was gradually heated in an oil bath to 130 °C until the solid dissolution and the stoichiometric amount of the amine (PEA, BZA, BrPEA, or FPEA) was added dropwise. Subsequently, a slow cooling down to room temperature at 1°C/5 min followed until the formation of a lamellar-shape bright pale-yellow product (for all the four perovskites). The precipitate was immediately filtered and dried at 65 °C under vacuum overnight. Samples have been stored in glovebox under argon atmosphere.

Single crystal X-ray diffraction:

Data at room temperature (λ = 0.71073 Å) for PEA_2GeBr_4 (CCDC 2084583), BZA_2GeBr_4 (CCDC 2084582) and $BrPEA_2GeBr_4$ (CCDC 2084581) were collected on a Bruker-Axs three-axis diffractometer equipped with the Smart-Apex CCD detector. Samples were quickly mounted and measured under nitrogen flux to avoid any sample oxidation. Omega-rotation frames were integrated with the SAINT software.[2] The absorption correction was performed with SADABS-2016/2.[3] Crystal structure was solved by direct methods as implemented in SIR 97 and refined using SHELXL-2018/3.[4,5] Anisotropic displacement parameters were refined for all non-hydrogen atoms. Hydrogens were placed at calculated positions with the appropriate AFIX instructions and refined using a riding model.

Crystal of PEA_2GeBr_4 resulted affected by twinning and the triclinic crystal structure was refined as a 2-component twin, with the twin law corresponding to a 180° rotation around the direction of the **b** unit cell edge. The PEA_2GeBr_4 compound were isostructural to the PEA_2SnBr_4 compound and the orientation of the triclinic unit cell adopted in literature was also used in our study.

Also the triclinic crystal of the BZA_2GeBr_4 resulted twinned and the crystal structure was refined as a 2-component twin, with the twin law defined as a 180° rotation around the [001] reciprocal-axis direction. Some of the C atoms of the eight independent organic moieties showed large and elongated atom displacement parameters, which produced inaccuracy on the C atom positions and short C_{ar}-C_{ar}

bond distances. Therefore, soft anti-bumping restraints (DFIX) were applied in the final refinement cycles, in order to obtain C_{ar}-C_{ar} bond distances of 1.39 ± 0.01 Å.

The orthorhombic non-centrosymmetric crystal structure of the $BrPEA_2GeBr_4$ compound was refined as a 2-component inversion twin. Moreover, extensive positional disorder affected the $GeBr_6$ octahedron, which resulted placed over alternative positions, mutually exclusive and occurring with the same statistical probability. The positional disorder was refined splitting both the atom site populated by the Ge specie and two of the four independent atom sites populated by the Br specie into two alternative and half populated positions.

Data collections at room temperature for $FPEA_2GeBr_4$ (CCDC 2084735) were performed using a Rigaku Oxford Diffraction SuperNova diffractometer equipped with a Dectris PILATUS3 R200K-A detector and a micro-focus sealed X-ray tube (λ = 0.71073 Å) X-ray diffraction intensity data were integrated with the CrysAlisPro package, while ABSPACK in CrysAlis RED was used for the absorption correction.[6] The structure was initially solved in the space group $P2_1/m$. However, no reasonable models were obtained in this centric space group mainly because of the presence of overlapping positions and structural disorder. Most of the atomic positions seemed to agree with the $P2_1/n$ space group requirements. At this stage, a careful analysis of the collected data showed that the $h0l$ reflections with con $h+l = 2n+1$ were present (due to a non-merohedric twinning) thus simulating the absence of the n glide. The structure was then solved and refined in the space group $P2_1/n$ using the program JANA2006.[7] For details on the averaging of equivalent reflections for twins in JANA2006, see for instance the appendix in Gaudin *et al.*.[8] After location of the heavy metal positions, the crystal structure was completed through successive difference-Fourier maps using *SHELXL* 2018/3.[5]

Data collections (λ = 0.71073 Å) at 100 K were performed using a Bruker Apex-II CCD diffractometer with the Bruker APEX2 program.[4,5] The Bruker SAINT software was used for integration and data reduction, while absorption correction was performed using SADABS-2016/2.[2,3] Crystal structures (CCDC 2084734, 2084736, 2084737) were solved and refined using *SHELXT* 2014/5 and *SHELXL* 2018/3.[9]

Synchrotron X-ray Powder Diffraction:

S-XRPD data were collected at 17 keV (λ= 0.72932 Å) on the high-resolution MCX beamline at the Elettra synchrotron light-source (Trieste, Italy) [doi:10.1002/zaac.201400163]. Finely ground powders were filled in 0.3 mm diameter borosilicate capillaries under moisture-free atmosphere (N_2 glove box with less than 1 ppm O_2 and H_2O) and sealed using a cutting torch. Capillaries were spun at 300 rpm and measured in Debye-Scherrer geometry on the 4-circles Huber goniometer using a

scintillator detector. Measurements at low temperature (100-300 K) were carried out by blowing a cold nitrogen stream using an Oxford Instruments cryojet while temperatures above 300 K were achieved using a hot-air gas-blower (Oxford Danfysik DGB-0002). A minimum of 5 minutes stabilization time was allowed before each measurement. Instrument profile was calculated using a silicon NIST standard (SRM 640c) and refining the peaks shape with the pseudo-Voigt (PV) function available in the GSAS-II suite [doi: 10.1107/S0021889813003531]. Data were then analyzed by means of Rietveld refinement using the structural models reported in the main text.

DSC Measurements:

Differential scanning calorimetry (DSC) analyses were performed by a Q2000 apparatus (TA Instruments, New Castle, DE, USA) by heating about 6 mg of powder in a close aluminum crucible from −80 °C to 80 °C (heating rate 5 K/min) and subsequent cooling down to -80°C under nitrogen flux (50 mL/min). Three independent measurements were taken on each sample. Crucibles have been prepared in the glovebox.

PL Measurements:

A Fluorolog 3 spectrofluorimeter (HORIBA Jobin-Yvon), equipped with a 450 W xenon lamp as exciting source and double grating excitation and emission monochromators was used for the PL measurements. All steady state optical measurements were performed at room temperature, at $l_{exc}=$ 370 nm and detected by a picosecond photon counter (TBX ps Photon Detection Module, HORIBA Jobin-Yvon).. The PL recombination dynamics were obtained by Time-Correlated Single Photon Counting (TCSPC) using a FluoroHub (HORIBA Jobin-Yvon) module and a laser diode emitting at 375 nm (NanoLED N375L, pulse width <200 ps, average power of 11pJ/pulse) with a repetition rate of 250 KHz as pulsed excitation source. Samples have been placed between two microscope slides and sealed with Kapton tape to protect them from air.

Computational methods:

First-principles calculations based on density functional theory (DFT) are carried out as implemented in the PWSCF Quantum-Espresso package.[10] Geometry optimization is performed using GGA-PBE level of theory and the electrons-ions interactions were described by ultrasoft pseudo-potentials with electrons from Br 4s, 4p; F 2s, 2p; N, C 2s, 2p; H 1s; Ge 4s, 4p, 3d; shells explicitly included in calculations.[11]

Band structures have been calculated using GGA-PBE level of theory.[11] DOS calculations have been performed by a single point hybrid calculations including SOC using the modified version of the

HSE06 functional including 43% Hartree-Fock exchange proposed in Ref. 5 with norm-conserving pseudo potentials with electrons from Br 4s, 4p; N, C 2s, 2p; H 1s; Sn 4s, 4p, 5s, 5p, 4d; shells explicitly included in calculations.[12,13]

The experimental cell parameters have been used in all the cases. Geometry optimizations are performed with a k-point sampling[7] of 4×4×1 along with plane-wave basis set cutoffs for the smooth part of the wave functions and augmented electronic density expansions of 25 and 200Ry, respectively.[14] HSE06-SOC calculation have been performed 1×1×1 k-point sampling with planewave basis set cutoffs for the smooth part of the wave functions and augmented electronic density expansions of 40 and 80Ry, respectively.

References

1 X. Li, J. M. Hoffman and M. G. Kanatzidis, *Chem. Rev.*, 2021, **121**, 2230–2291.

2 *Bruker. SAINT*, Bruker AXS Inc., 2015.

3 L. Krause, R. Herbst-Irmer, G. M. Sheldrick and D. Stalke, *J Appl Cryst*, 2015, **48**, 3–10.

4 A. Altomare, M. C. Burla, M. Camalli, G. L. Cascarano, C. Giacovazzo, A. Guagliardi, A. G. G. Moliterni, G. Polidori and R. Spagna, *Journal of Applied Crystallography*, 1999, **32**, 115–119.

5 G. M. Sheldrick, *Acta Cryst C*, 2015, **71**, 3–8.

6

7 V. Petříček, M. Dušek and L. Palatinus, *Zeitschrift für Kristallographie - Crystalline Materials*, , DOI:10.1515/zkri-2014-1737.

8 E. Gaudin, V. Petricek, F. Boucher, F. Taulelle and M. Evain, *Acta Crystallographica Section B*, 2000, **56**, 972–979.

9 G. M. Sheldrick, *Acta Crystallographica Section A*, 2015, **71**, 3–8.

10 P. Giannozzi, S. Baroni, N. Bonini, M. Calandra, R. Car, C. Cavazzoni, D. Ceresoli, G. L. Chiarotti, M. Cococcioni, I. Dabo, A. D. Corso, S. de Gironcoli, S. Fabris, G. Fratesi, R. Gebauer, U. Gerstmann, C. Gougoussis, A. Kokalj, M. Lazzeri, L. Martin-Samos, N. Marzari, F. Mauri, R. Mazzarello, S. Paolini, A. Pasquarello, L. Paulatto, C. Sbraccia, S. Scandolo, G. Sclauzero, A. P.

Seitsonen, A. Smogunov, P. Umari and R. M. Wentzcovitch, *Journal of Physics: Condensed Matter*, 2009, **21**, 395502.

11 J. P. Perdew, K. Burke and M. Ernzerhof, *Phys. Rev. Lett.*, 1996, **77**, 3865–3868.

12 J. Heyd, G. E. Scuseria and M. Ernzerhof, *The Journal of Chemical Physics*, 2003, **118**, 8207–8215.

13 M.-H. Du, *J. Phys. Chem. Lett.*, 2015, **6**, 1461–1466.

14 H. J. Monkhorst and J. D. Pack, *Phys. Rev. B*, 1976, **13**, 5188–5192.